
RealEngine: Simulating Autonomous Driving in Realistic Context

Junzhe Jiang¹ Nan Song¹ Jingyu Li¹ Xiatian Zhu² Li Zhang^{1*}

¹School of Data Science, Fudan University ²University of Surrey

<https://github.com/fudan-zvg/RealEngine>

Abstract

Driving simulation plays a crucial role in developing reliable driving agents by providing controlled, evaluative environments. To enable meaningful assessments, a high-quality driving simulator must satisfy several key requirements: multi-modal sensing capabilities (e.g., camera and LiDAR) with realistic scene rendering to minimize observational discrepancies; closed-loop evaluation to support free-form trajectory behaviors; highly diverse traffic scenarios for thorough evaluation; multi-agent cooperation to capture interaction dynamics; and high computational efficiency to ensure affordability and scalability. However, existing simulators and benchmarks fail to comprehensively meet these fundamental criteria. To bridge this gap, this paper introduces *RealEngine*, a novel driving simulation framework that holistically integrates 3D scene reconstruction and novel view synthesis techniques to achieve realistic and flexible closed-loop simulation in the driving context. By leveraging real-world multi-modal sensor data, *RealEngine* reconstructs background scenes and foreground traffic participants separately, allowing for highly diverse and realistic traffic scenarios through flexible scene composition. This synergistic fusion of scene reconstruction and view synthesis enables photorealistic rendering across multiple sensor modalities, ensuring both perceptual fidelity and geometric accuracy. Building upon this environment, *RealEngine* supports three essential driving simulation categories: non-reactive simulation, safety testing, and multi-agent interaction, collectively forming a reliable and comprehensive benchmark for evaluating the real-world performance of driving agents.

1 Introduction

Autonomous driving (AD) methods [1, 2, 3, 4, 5, 6] have advanced rapidly, largely due to the introduction of diverse driving datasets [7, 8, 9] and simulators [10]. These resources facilitate research by supporting model training, testing, and evaluation across a variety of virtual and real driving environments, utilizing a wealth of multimodal sensor, including cameras and LiDAR.

However, existing AD datasets and simulators have fundamental limitations that prevent them from fully capturing real-world driving scenarios and challenges, diminishing their credibility and usefulness in practical applications. For instance, real driving data typically provides only pre-existing driving trajectories [7, 8], allowing for open-loop evaluation without immediate feedback or interaction with the trajectories planned by driving agents. This results in a significant discrepancy between simulated and actual driving behavior. The static nature of recorded datasets, where other vehicles do not react to the actions of the ego vehicle, creates a scenario fundamentally different from real-world situations. Although the closed-loop simulator CARLA [10] addresses this issue by providing real-time feedback to driving agents, it relies on manual 3D modeling and

*Corresponding author (lizhangfd@fudan.edu.cn).

Table 1: Comparison of various datasets, generative models, world models, and simulators in terms of interactivity, fidelity, diversity, and efficiency. **DATA.** represents dataset, **GEN.** represents generative model, **W.M.** represents world model, **SIM.** represents simulator.

Type	Name	Interactivity			Fidelity		Diversity			Efficiency
		Uncontrollable closed-loop	Controllable closed-loop	Multi-agent simulation	Realistic images	Real-world roadgraph	Safety test cases	Multi-view images	LiDAR point cloud	Efficient rendering
DATA.	CitySim [17] / NGSIM [18]	✗	✗	✗	✗	✓	✗	✗	✗	✗
	Bench2Drive [19]	✗	✗	✗	✗	✗	✓	✗	✓	✓
	nuPlan [7] / Navsim [20]	✗	✗	✗	✓	✓	✗	✓	✓	✗
	nuScenes [8] / Waymo dataset [21]	✗	✗	✗	✓	✓	✗	✓	✓	✗
GEN.	MagicDrive [22] / DriveDreamer [23]	✗	✗	✗	✓	✓	✗	✓	✗	✗
	SimGen [24]	✗	✗	✗	✓	✓	✗	✗	✗	✗
W.M.	KiGRAS [25] / SMART [26]	✓	✗	✓	✗	✓	✗	✗	✗	✗
	MUVO [27]	✓	✗	✗	✗	✓	✗	✗	✓	✗
	Vista [28] / GAIA-1 [29]	✓	✗	✗	✓	✗	✗	✗	✗	✗
SIM.	Waymax [30]	✓	✓	✓	✗	✓	✗	✗	✗	✗
	SUMO [31] / LimSim [32]	✓	✓	✗	✗	✓	✗	✗	✗	✗
	CARLA [10]	✓	✓	✗	✗	✓	✗	✓	✓	✗
	STRIVE [33]	✓	✓	✗	✗	✓	✓	✗	✗	✗
	MetaDrive [34]	✓	✓	✗	✗	✓	✓	✗	✗	✓
	Unisim [35] / OASim [36]	✓	✓	✗	✓	✓	✗	✓	✓	✗
	NeuroNCAP [37]	✓	✓	✗	✓	✓	✓	✓	✗	✗
	DriveArena [38]	✓	✓	✗	✓	✓	✗	✓	✗	✗
	HUGSIM [39]	✓	✓	✓	✓	✓	✓	✓	✗	✗
	<i>RealEngine (Ours)</i>	✓	✓	✓	✓	✓	✓	✓	✓	✓

graphics engines, which lacks realism and exhibits a substantial appearance gap from actual driving scenarios. Consequently, models trained in this environment may struggle to handle real-world driving conditions effectively. Further, previous benchmarks primarily focus on non-collision and normal driving scenarios, which limits the models’ ability to address unseen risks encountered in the real world.

To advance the field, we introduce *RealEngine*, a pioneering autonomous driving simulation platform capable of rendering realistic multimodal sensor data efficiently and supporting closed-loop simulation. It is distinguished by the following features: **(i) Realistic scene rendering**, closely resembling the real world to minimize domain discrepancies between simulated and actual driving environments, allowing both camera images and LiDAR point clouds; **(ii) Closed-loop simulation**, enabling driving along free-form trajectories planned by agents while providing corresponding feedback; **(iii) Supporting diverse scenarios**, including a wide range of hazardous driving situations to facilitate comprehensive safety-critical evaluations of driving agents; **(iv) Multi-agent co-operation and interaction**, closely approximating various real-world conditions in terms of driving dynamics and scene complexity. As summarized in Table 1, no existing benchmarks or simulators meet these fundamental requirements simultaneously, as well as a spectrum of driving simulation focused features.

Our *RealEngine* is founded on the innovative concept of seamlessly integrating scene reconstruction with the composition of traffic participants. We reconstruct the background scene and foreground traffic participants separately with the corresponding real-world data. This approach simultaneously addresses key limitations of existing scene reconstruction methods [11, 12, 13, 14, 15, 16]: **(i)** Unable to acquire occluded regions within a scene; **(ii)** Inferior performance in synthesizing novel viewpoints of traffic participants; **(iii)** Limited choice of possible traffic participants. Our decomposed design naturally supports flexible scene editing while enabling the concurrent operation of multiple driving agents, as required for realistic driving simulations. By merging the background scene with diverse traffic participants, we can efficiently simulate a wide range of high-quality, unique driving scenarios tailored to any specific requirements. We generate a diverse range of driving scenarios and simulate three driving categories: *non-reactive*, *safety test*, and *multi-agent interaction*. This offers a high quality, reliable, flexible, and comprehensive benchmark for assessing the real-world performance of driving agents.

2 Related work

Autonomous driving. Recent research in autonomous driving have shifted from addressing individual tasks to exploring end-to-end planning, enabling the progressive execution from perception to ego-planning within a unified framework. Early works [40, 41, 42] implement this by leveraging simplified auxiliary tasks, which limits the final performance. In contrast, UniAD [4] and VAD [43] have advanced this paradigm by integrating a broader spectrum of driving tasks, achieving notable progress in planning tasks by producing explicit intermediate results. Additionally, recent approaches present

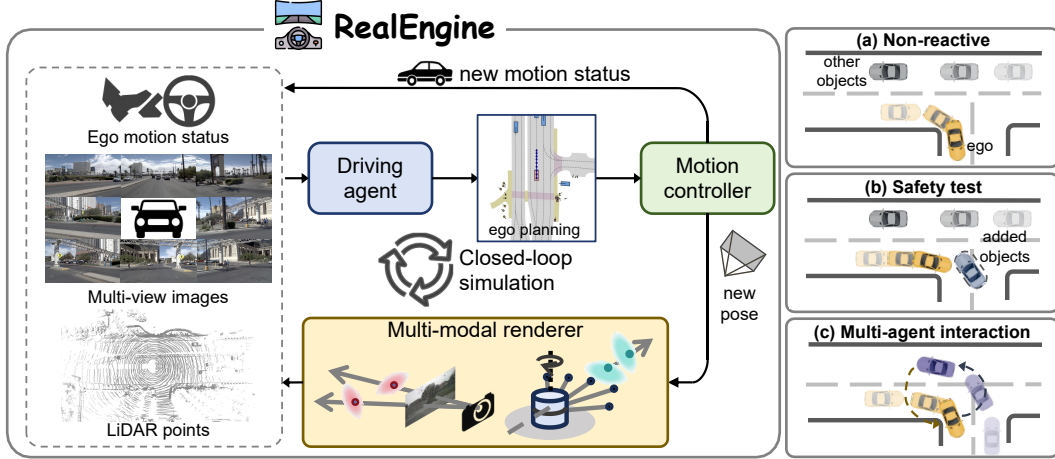


Figure 1: **The working mechanism of *RealEngine*.** It consists of three modules: a driving agent, a motion controller and a multi-model renderer. Given a traffic scene represented by multimodal data including multi-view images and LiDAR point cloud, the driving agent predicts the trajectory, according to which *RealEngine* updates the ego-motion state for all traffic participants. Moving to the next time step, the multimodal sensor data will be refreshed by the current ego-motion state, which is then used for the driving agent to make the next trajectory planning. We consider three driving situations: non-reactive, safety test, and multi-agent interaction.

sparse representations [44, 45], employ lightweight diffusion-based generation [46] to efficiently facilitate end-to-end planning. For enabling these driving methods to be evaluated extensively and authentically, we provide a reliable testing platform here.

Sensor simulation. The geometric reconstruction of extensive urban spaces, such as streets and cities, has played a pivotal role in autonomous driving [21, 47, 8]. Recently, Gaussian splatting [48] based methods have been introduced to model dynamic urban scenes. PVG [11] incorporates periodic vibration at each Gaussian primitive to represent static and dynamic objects uniformly. At the same time, explicitly decomposing scenes into independent entities has become common practice, as seen in works such as StreetGaussians [14], DrivingGaussians [49], HUGS [50] and OmniRe [15]. Recently, LiDAR simulation studies have focused on using real data for improved realism. For instance, LiDARsim [51] and PCGen [52] use multi-step, data-driven methods to simulate point clouds from real data. Additionally, works such as [53, 54, 55, 56, 57, 58] leverage NeRF [59] for scene reconstruction and LiDAR simulation. Recent works [60, 61] introduce Gaussian splatting [48] into the LiDAR reconstruction task, achieving improved reconstruction quality and rendering speed. However, sensor-acquired data is prone to occlusions, leading to information loss within scenes. Additionally, reconstructed dynamic objects can distort when viewed from alternative perspectives, limiting scene editability and novel view synthesis. To address these challenges, we propose modeling the foreground and background separately allowing them to be composed in a flexible manner, resulting in a comprehensive driving simulation platform.

Closed-loop simulation in realistic settings. Closed-loop simulation [30, 7, 10, 34] is crucial for the evaluation and deployment of AD planning systems, collecting sufficient driving statistics and improving the emergency response capability of driving agents. To make simulators more realistic, recent research has explored using existing real-world driving datasets. Bench2Drive [19] improves the CARLA benchmark by reconstructing the data format to be more aligned with the nuScenes dataset, bridging the gap between reinforcement learning planners and end-to-end planners. Navsim [20] imitates closed-loop evaluation to adjust the nuPlan benchmark, introducing more comprehensive and practical metrics. With the emergence of novel 3D rendering and generation research, some works integrate these techniques into existing datasets, better simulating and constructing richer and more diverse scenarios. NeuroNCAP [37] utilizes NeRF [59] to render novel surrounding views and creates collision scenarios to enhance measurement. Relying on powerful generative models and extensive driving data, DriveArena [38] is capable to yield controllable and abundant real-world scenarios and realize closed-loop simulation. However, these simulators all fail to meet the fundamental criteria as mentioned earlier. This motivates the introduction of our *RealEngine*, a more reliable and powerful benchmark for assessing the real-world performance of driving agents.

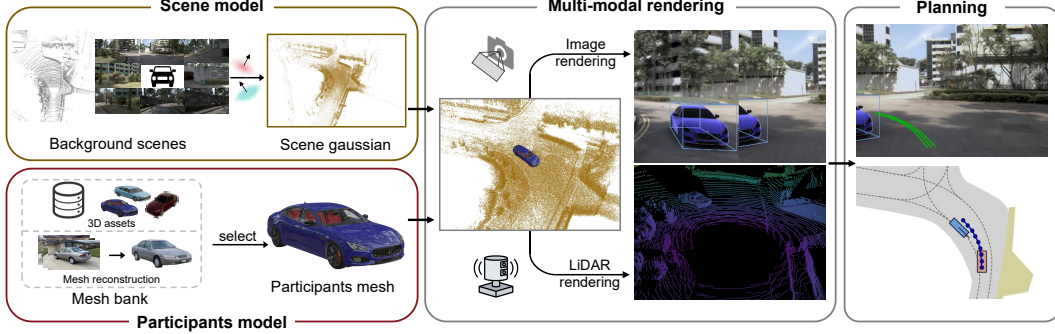


Figure 2: **Scene composition.** We start with modeling the background scene based on real sensor data and obtaining the meshes of traffic participants either by extracting them from the reconstructed data or through manual creation. That makes a rich space for designing a variety of customizable traffic scenarios. To create a specific scenario, we select both the background scene and traffic participants, which can be integrated based on each participant’s spatial coordinates over time. This naturally enables the creation of highly diverse scenes to support extensive closed-loop simulation.

3 Method

We present *RealEngine*, a reliable and comprehensive autonomous driving simulation platform capable of rendering realistic multimodal sensor data efficiently and supporting closed-loop simulation. It is composed of: (i) Simulator infrastructure including background scene and traffic participants as well as their compositions; (ii) Closed-loop driving simulation; (iii) Assessment of driving agents. The working mechanism of *RealEngine* is depicted in Figure 1.

3.1 Simulator infrastructure

The advancement of recent generative models has been recently exploited for closed-loop driving simulation. For example, DriveArena [38] streamlines a couple of generative functions, such as interactive traffic flows and novel scene synthesis, allowing to simulate virtual driving scenes. However, this approach suffers from several key drawbacks: (1) Need for large manually labelled training data for video generative model optimization; (2) Substantial running overhead, even without support to multimodal sensor data such as LiDAR point clouds (3) Inability to support multi-agent co-operation and interaction. (4) Dependence on a pre-defined high-definite map; (5) Low controllability on the traffic scenario including background scene and traffic participants, consequently causing frequent situational inconsistency over space and time; (6) Low spatiotemporal realism. While some of the above issues, such as realistic scene rendering, more flexible traffic scenario editing, and no need for training data collection, can be addressed by NeuroNCAP [37], it narrowly focuses on safety test of driving agents. Further, it cannot well generalize to free form trajectories otherwise the novel view synthesis will degraded substantially.

To address all the problems mentioned above, we propose decoupling the background scene and foreground traffic participants by reconstructing each of them individually from the corresponding real sensor data, allowing the composition of diverse traffic scenarios and free form driving trajectories of multiple agents while maintaining high-fidelity novel view synthesis in multiple modalities (e.g., camera images and LiDAR).

3.1.1 Background scene models

To reconstruct realistic background environments, we adopt StreetGaussians [14] for camera images and GS-LiDAR [60] for LiDAR point clouds, chosen for their high rendering efficiency and cross-modal fidelity. Importantly, RealEngine maintains flexibility—alternative methods such as PVG [11], OmniRe [15], and LiDAR-RT [61] can be seamlessly incorporated into our system as modular components.

Pose calibrations in nuPlan [7] is relatively coarse, posing challenges for accurate scene reconstruction. A widely used conventional method for camera pose correction [14, 15, 62] involves learning a trainable correction matrix that adjusts the camera pose automatically during training. However,

this method is only effective for small pose deviations and fails to converge on nuPlan, leading to suboptimal results. To address this issue, we propose a pose correction method based on LiDAR point cloud registration.

As the geometric information of the background scene remains fixed in the world coordinate system, we can align the ego vehicle’s poses across different frames by registering LiDAR points transformed to the world. We remove dynamic vehicles from the LiDAR data based on annotation information and filter out ground points which vary significantly across frames. All remaining point clouds are transformed into the world coordinate system and truncated within a predefined region to ensure consistency across frames. We select the central LiDAR frame $\mathbf{P}_{\text{refer}}$ as the reference frame and apply a learnable correction matrix \mathbf{M} to transform the LiDAR frames \mathbf{P} . The transformed LiDAR frames are then compared with the reference frame using the Chamfer Distance (C-D) [63] as the loss function:

$$\mathcal{L}_{\text{cd}} = \text{CD}(\mathbf{M}\mathbf{P}, \mathbf{P}_{\text{refer}}) \quad (1)$$

Additionally, we leverage learnable image exposure transformations to handle cross-camera appearance variations, and utilizes video generative prior [64, 65] to optimize the scene model across multiple trajectories in Appendix A.2. For further details on camera image and LiDAR point cloud reconstruction, please refer to Appendix A. By leveraging these advanced reconstruction techniques, we achieve precise multi-modal background reconstruction with high rendering efficiency, enabling flexible scene editing and realistic simulation of autonomous driving agents.

3.1.2 Traffic participants models

Traffic participants (e.g., vehicles, bicycles) are essential for realistic driving scenarios. To enable high-fidelity and diverse simulations, we curate a comprehensive set of 3D participant models. Conventional approaches [14, 15, 39] insert reconstructed Gaussian splatting primitives into the background scene according to predefined trajectories. While providing high-quality rendering from training viewpoints, they degrade significantly when rendering resolution, viewpoint, or object distance changes [66, 67, 68]. This degradation causes visual artifacts, especially in close-range interactions (e.g., collisions), and also introduces inconsistencies in lighting and shadows between foreground objects and the background scene.

To address these issues, RealEngine represents traffic participants using 3D meshes, ensuring consistent geometry across all viewpoints and distances. To achieve seamless integration, we employ a diffusion model to guide learning of scene-consistent lighting and shading, as further detailed in Section 3.1.3. Meshes are rendered using ray tracing to produce both RGB images and depth maps, enabling accurate occlusion reasoning between participants and scenes.

The 3D meshes are sourced from two complementary pipelines: (i) High-quality meshes manually created for key traffic objects. (ii) Meshes reconstructed from real-world datasets, including 360-degree images from CO3D [69] and 3DRealCar [70]. These are processed via 3D Gaussian Splatting (3DGS) for reconstruction, followed by mesh extraction for flexible use in scene composition.

3.1.3 Driving scenario composition

The combination of reconstructed background scenes and traffic participant models forms a rich design space for creating diverse and flexible driving scenarios. Scenario composition begins by selecting a background scene, into which a set of traffic participants is inserted. Each participant is assigned an initial position, orientation, and free-form trajectory, either manually specified or dynamically planned by a driving agent. These participants are then spatially registered into the background scene’s coordinate system. An overview is shown in Figure 2.

To ensure realistic integration between foreground participants and background scenes, we introduce a physically based rendering (PBR) process that optimizes environment light maps for consistent relighting and shadow casting. We adopt the Disney BRDF lighting model [71], where the foreground color is computed as:

$$\mathbf{C}_{fg}(\mathbf{x}) = \int_{\Omega} f_r(\mathbf{x}, \boldsymbol{\omega}, \boldsymbol{\omega}_o) \mathbf{L}_i(\boldsymbol{\omega}) |\langle \boldsymbol{\omega}, \mathbf{n} \rangle| d\boldsymbol{\omega} \quad (2)$$

Here, \mathbf{x} denotes the surface point where the camera ray $\boldsymbol{\omega}_o$ intersects, \mathbf{n} the surface normal, $\boldsymbol{\omega}$ the light direction, and \mathbf{L}_i the incoming illumination. The BRDF f_r models the surface reflectance.

For shadows, we assume a ground plane closely aligned to the foreground object’s base. For each camera ray ω_o , we compute the ground intersection x' and its normal n' . Shadow rays ω' are traced across the hemisphere Ω' to determine occlusion, and the shadow intensity I is computed:

$$I(x') = \frac{\int_{\Omega(x')} L_s(\omega') |\langle \omega', n' \rangle| d\omega'}{\int_{\Omega'} L_s(\omega') |\langle \omega', n' \rangle| d\omega'} \quad (3)$$

where L_s is the shadow environment map, and $\Omega(x')$ represents the solid angle of unoccluded light rays at point x' with respect to the foreground mesh.

The final composed image is:

$$C = C_{bg} \cdot I \cdot (1 - M_{fg}) + C_{fg} \cdot M_{fg} \quad (4)$$

where C_{bg} is the background image, C_{fg} and M_{fg} are the rendered foreground RGB and mask, respectively. We optimize $\{L_i, L_s\}$ using StableDiffusion [72] with SDS loss [73], ensuring photorealistic blending.

3.2 Closed-loop driving simulation

Built upon this flexible scenario composition and novel view synthesis-enabled reconstruction, RealEngine supports a wide range of driving scenarios. We demonstrate three representative categories:

Non-reactive Simulation. Evaluates closed-loop planning where other participants follow fixed pre-recorded trajectories (Figure 1 (a)). The agent perceives rendered multi-modal sensor data, plans trajectories, and executes motion via a linear quadratic regulator (LQR), completing the closed-loop cycle.

Safety Test Simulation. Evaluates agent reactions to inserted participants exhibiting hazardous behaviors (e.g., sudden lane changes or blocked intersections), testing safety-critical skills (Figure 1 (b)).

Multi-agent Interaction Simulation. Simulates cooperative and adversarial interactions where multiple agents, each running independent planning, simultaneously navigate the scene (Figure 1 (c)).

3.3 Assessment of driving agents

Driving agent assessment aims to evaluate the agent’s trajectory planning performance across both space and time, considering safety, progress, and interaction quality within diverse traffic scenarios. In traditional open-loop evaluation, the Predictive Driver Model Score (PDMS) [20] measures trajectory quality at individual time steps. However, open-loop PDMS does not capture how planning decisions evolve over time, nor does it account for interactions with dynamic participants in the scene.

To address these issues, RealEngine introduces a *closed-loop extension* of PDMS, which evaluates the agent’s performance over a continuous sequence of future steps. Specifically, starting at time step t , the agent plans a sequence of future positions over N steps, continuously interacting with the environment and surrounding participants.

At each step, the agent receives updated sensor observations rendered from the new position, which are used to generate the next planned trajectory, creating a fully closed-loop simulation. During this process, other traffic participants follow either their pre-recorded reference trajectories or react through independent planning processes, depending on the scenario type.

The final closed-loop PDMS over the horizon t to $t + N$ is formulated as:

$$\text{PDMS}_{t:t+N} = \underbrace{\left(\prod_{m \in \{\text{NC}, \text{DAC}\}} \text{score}_m \right)}_{\text{penalty terms}} \times \underbrace{\left(\frac{\sum_{w \in \{\text{EP}, \text{TTC}, \text{C}\}} \text{weight}_w \cdot \text{score}_w}{\sum_{w \in \{\text{EP}, \text{TTC}, \text{C}\}} \text{weight}_w} \right)}_{\text{weighted average rewards}}. \quad (5)$$

The *penalty terms* include: (1) NC (No Collision): Whether the agent avoids collisions with other vehicles, pedestrians, or cyclists. (2) DAC (Drivable Area Compliance): Whether the agent stays within the valid drivable area (lanes, intersections, etc.).



Figure 3: (a) Compared to state-of-the-art reconstruction methods, we achieve superior camera image reconstruction in the nuPlan [7] benchmark. Additionally, (b) our foreground relighting technique enables seamless integration of inserted participants with the background scene.

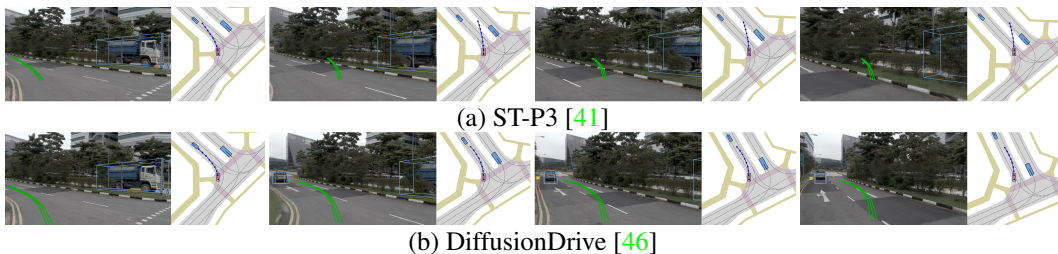


Figure 4: **Non-reactive simulation.** The driving agent’s planned trajectory at each step is visualized in bird’s-eye view (blue) and the front-view camera (green). During closed-loop simulation, ST-P3 [41] exhibits inconsistencies in consecutive frame planning, leading to error accumulation and causing the vehicle to navigate into invalid regions. In contrast, DiffusionDrive [46] maintains more consistent planning across consecutive frames, resulting in a higher PDM Score.

The *weighted average reward terms* reflect the overall driving quality across three dimensions: (1) EP (Ego Progress): How effectively the agent advances toward the goal within the given time horizon. (2) TTC (Time to Collision): How much time the agent maintains between itself and potential collision risks. (3) C (Comfort): Evaluating smoothness of the planned trajectory, including acceleration and jerk. This combined metric captures both safety-critical behaviors (penalties) and desirable driving qualities (rewards), providing a comprehensive assessment of the agent’s closed-loop performance in diverse and dynamic traffic scenarios.

4 Experiments

Datasets. We use CO3D [69] and 3DRealCar [70] to reconstruct diverse foreground traffic participants, followed by mesh extraction for rendering and scene composition. Additionally, we include high-quality meshes from Sketchfab [74] for further diversity in foreground insertion and relighting.

For background scene reconstruction and scene editing, we leverage Navsim [20], which is derived from OpenScene [75], a simplified version of nuPlan [7]. We select 14 diverse sequences from Navsim for scene editing and driving agent evaluation, and design 14, 21, and 14 test cases for the non-reactive, safety, and multi-agent interaction simulation, respectively. To ensure high-quality sensor simulation, we retrieve high-frequency images and LiDAR point clouds from the corresponding nuPlan sequences for background scene reconstruction. Using an NVIDIA RTX A6000, the rendering frame rate reaches 30Hz for camera images and 15Hz for LiDAR data.

Autonomous driving models. We evaluate four end-to-end driving models: ST-P3 [41], VAD [43], TransFuser [42], and DiffusionDrive [46], with ST-P3 and VAD reimplemented on nuPlan [7] for consistency. As a baseline, we also test Navsim’s constant velocity model for comparison.

4.1 Driving scenario quality

We compared our optimized reconstruction results (Appendix A) with the state-of-the-art methods [14, 15, 11] on 6 Navsim [20] sequences, as shown in Figure 3 (a) and Table 3, and observed a notable improvement in the reconstruction performance on nuPlan. Meanwhile, our foreground insertion

Table 2: **Non-reactive simulation.** We show the no at-fault collision (NC), drivable area compliance (DAC), time-to-collision (TTC), comfort (Comf.), and ego progress (EP) subscores, and the PDM Score (PDMS), as percentages.

Method	Loop	Ego stat.	Image	LiDAR	NC ↑	DAC ↑	TTC ↑	Comf. ↑	EP ↑	PDMS ↑
Constant velocity [20]		✓			92.9	64.3	85.7	100	29.4	46.8
ST-P3 [41]	Open-loop	✓	✓		92.9	71.4	92.9	100	46.2	59.6
VAD [43]		✓	✓		92.9	85.7	92.9	100	48.5	66.1
TransFuser [42]		✓	✓	✓	92.9	85.7	92.9	100	55.9	69.1
DiffusionDrive [46]		✓	✓	✓	92.9	85.7	92.9	100	56.7	69.5
ST-P3 [41]	Closed-loop	✓	✓		100	64.3	85.7	100	35.6	47.5
VAD [43]		✓	✓		85.7	78.6	78.6	100	34.3	53.0
TransFuser [42]		✓	✓	✓	92.9	71.4	85.7	100	46.0	57.9
DiffusionDrive [46]		✓	✓	✓	92.9	71.4	92.9	100	47.1	61.3
Human					100	100	92.9	100	68.3	83.8

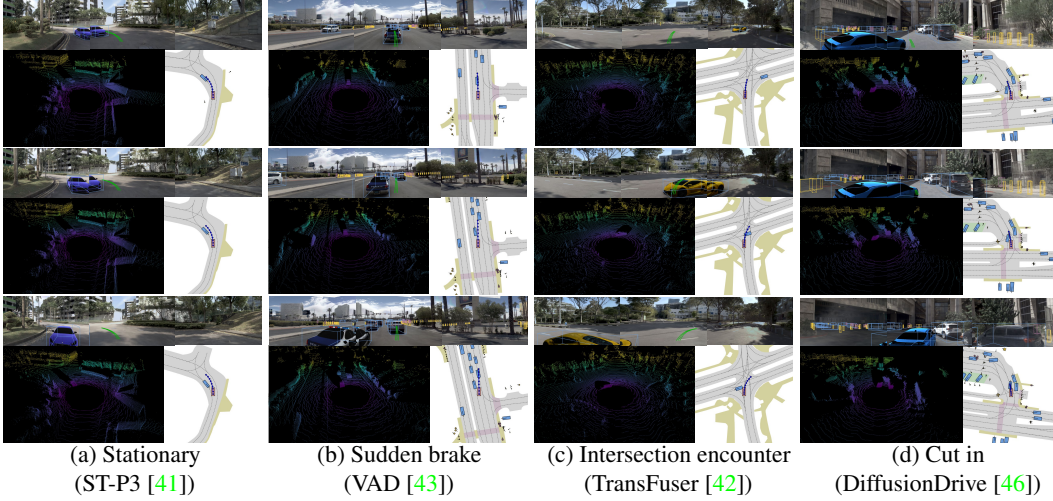


Figure 5: **Safety test simulation.** The driving agent’s planned trajectory at each step is visualized in bird’s-eye view (blue) and the front-view camera (green). The driving agent is navigating in our designed safety-critical scenarios. The agent may (a)(b) successfully avoid a collision, (c) exhibit no reaction, or (d) attempt to decelerate to prevent a collision but ultimately fail.

blends more harmoniously with the background and can be recognized by perception models [76, 77, 78], as shown in Figure 3 (b). This enables the driving agents to correctly recognize the inserted foreground participants and respond accordingly.

Table 3: Comparison with state-of-the-art camera images reconstruction methods in the nuPlan benchmark.

	PSNR↑	SSIM↑	LPIPS↓
StreetGaussians [14]	26.02	0.798	0.179
Omnire [15]	26.89	0.837	0.165
PVG [11]	28.32	0.854	0.176
RealEngine(Ours)	29.67	0.897	0.093

4.2 Closed-loop simulation

Non-reactive simulation. In the non-reactive setting, we conduct open-loop and closed-loop simulations on the driving agents and compare their performance, as shown in Table 2. Compared to directly predicting multiple frame trajectories in open-loop simulation, the PDM Score of the continuously predicted trajectories by the driving agent in closed-loop simulation is reduced to varying degrees. In particular, models tend to exhibit inconsistency in the adjacent predicted trajectories. This inconsistency leads to cumulative errors, causing the vehicle to navigate to unreasonable areas and resulting in a decrease in the DAC (drivable area compliance) metric, as shown in Figure 4.

Safety test simulation. For safety test simulation, we designed three test cases (simple, moderate, and challenging) tailored to each specific scenario and conducted closed-loop simulations to compute

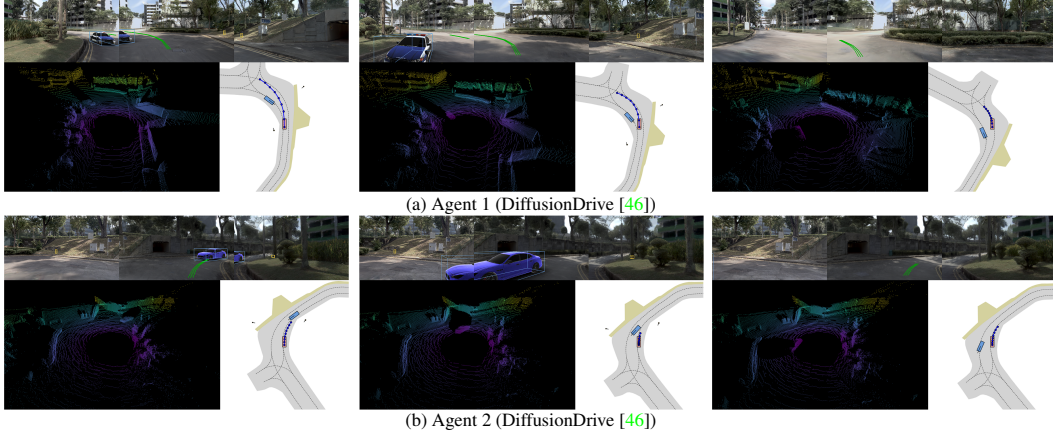


Figure 6: **Multi-agent interaction simulation.** The trajectory annotations are consistent with Figure 5. We set two agents (DiffusionDrive [46]) to plan trajectories simultaneously and independently in the showed turning scenario. The first agent avoids collision by increasing its turning radius, while the second agent decelerates to allow safe passage. Once the vehicles have passed each other, the second agent resumes its original speed.

Table 4: **Safety test and multi-agent simulation.** The notations are consistent with the **non-reactive simulation** Table 2 above.

Method	Simulation	Ego stat.	Image	LiDAR	NC \uparrow	DAC \uparrow	TTC \uparrow	Comf. \uparrow	EP \uparrow	PDMS \uparrow
Constant velocity [20]	Safety test	\checkmark			47.6	71.4	38.1	100	36.7	36.3
ST-P3 [41]		\checkmark	\checkmark		47.6	100	42.9	100	44.7	44.4
VAD [43]		\checkmark	\checkmark		47.6	95.2	28.6	100	41.2	37.0
TransFuser [42]		\checkmark	\checkmark	\checkmark	47.6	100	38.1	100	44.1	42.2
DiffusionDrive [46]		\checkmark	\checkmark	\checkmark	57.1	100	52.4	100	54.0	53.8
Constant velocity [20]	Multi-agent	\checkmark			42.8	60.7	39.3	100	27.8	27.4
ST-P3 [41]		\checkmark	\checkmark		53.6	96.4	50.0	100	44.6	46.3
VAD [43]		\checkmark	\checkmark		32.1	71.4	32.1	100	27.7	28.8
TransFuser [42]		\checkmark	\checkmark	\checkmark	60.7	96.4	53.6	100	54.3	55.0
DiffusionDrive [46]		\checkmark	\checkmark	\checkmark	57.1	96.4	50.0	100	51.7	51.9

the PDM Score. As shown in Figure 5, in simple and moderate scenarios, such as a stationary vehicle blocking the lane or a sudden brake, driving agents can reasonably maneuver to avoid collisions. However, in more challenging scenarios, such as aggressive lane changes or intersection encounters, driving agents may exhibit some reaction but fail to avoid collisions, or in some cases, show minimal response to an imminent collision, leading to a significant drop in the PDM Score, as shown in Table 4.

Multi-agent interaction simulation. In the multi-agent interaction simulation, each vehicle is assigned to an instance of a certain driving agent model for independent and simultaneous control, with only the initial speed and high-level driving commands (right, left, straight, or unknown) specified. For each specific scenario, we design both simple and challenging test cases. At each time step, we render the sensor data for all driving agents to plan trajectories and conduct closed-loop simulations to compute the PDM scores for all instances and average the results, as presented in Table 4. Additionally, Figure 6 illustrates a turning scenario involving two DiffusionDrive [46] instances, where both agents successfully avoid collisions by adopting different yet reasonable strategies.

5 Conclusion

This paper introduces a novel driving simulation platform, *RealEngine*, capable of rendering realistic multimodal sensor data efficiently and perform closed-loop simulation in highly diverse traffic scenarios. *RealEngine* employs a foreground-background separate reconstruction and composition rendering approach, enabling convenient and more flexible control and editing of scenes. This allows for realistic interaction and continuous feedback between the driving agent and the simulation platform, while also facilitating multi-agent interactions within the simulation. Based on this, we simulate three driving categories: non-reactive, safety test, and multi-agent interaction, to establish a reliable and comprehensive benchmark for evaluating the real-world performance of driving agents.

References

- [1] Tianwei Yin, Xingyi Zhou, and Philipp Krahenbuhl. Center-based 3d object detection and tracking. In *CVPR*, 2021. 1
- [2] Xin Li, Botian Shi, Yuenan Hou, Xingjiao Wu, Tianlong Ma, Yikang Li, and Liang He. Homogeneous multi-modal feature fusion and interaction for 3d object detection. In *ECCV*, 2022. 1
- [3] Tengju Ye, Wei Jing, Chunyong Hu, Shikun Huang, Lingping Gao, Fangzhen Li, Jingke Wang, Ke Guo, Wencong Xiao, Weibo Mao, et al. Fusionad: Multi-modality fusion for prediction and planning tasks of autonomous driving. *arXiv preprint*, 2023. 1
- [4] Yihan Hu, Jiazhi Yang, Li Chen, Keyu Li, Chonghao Sima, Xizhou Zhu, Siqu Chai, Senyao Du, Tianwei Lin, Wenhai Wang, et al. Planning-oriented autonomous driving. In *CVPR*, 2023. 1, 2
- [5] Licheng Wen, Daocheng Fu, Xin Li, Xinyu Cai, Tao Ma, Pinlong Cai, Min Dou, Botian Shi, Liang He, and Yu Qiao. Dilu: A knowledge-driven approach to autonomous driving with large language models. *arXiv preprint*, 2023. 1
- [6] Daocheng Fu, Xin Li, Licheng Wen, Min Dou, Pinlong Cai, Botian Shi, and Yu Qiao. Drive like a human: Rethinking autonomous driving with large language models. In *WACV*, 2024. 1
- [7] K. Tan et al. H. Caesar, J. Kabzan. Nuplan: A closed-loop ml-based planning benchmark for autonomous vehicles. In *CVPR ADP3 workshop*, 2021. 1, 2, 3, 4, 7, 15
- [8] Holger Caesar, Varun Bankiti, Alex H Lang, Sourabh Vora, Venice Erin Liong, Qiang Xu, Anush Krishnan, Yu Pan, Giancarlo Baldan, and Oscar Beijbom. nuscenes: A multimodal dataset for autonomous driving. In *CVPR*, 2020. 1, 2, 3
- [9] Nico Montali, John Lambert, Paul Mougin, Alex Kuefler, Nicholas Rhinehart, Michelle Li, Cole Gulino, Tristan Emrich, Zoey Yang, Shimon Whiteson, et al. The waymo open sim agents challenge. *NeurIPS*, 2024. 1
- [10] Alexey Dosovitskiy, German Ros, Felipe Codevilla, Antonio Lopez, and Vladlen Koltun. Carla: An open urban driving simulator. In *CoRL*, 2017. 1, 2, 3
- [11] Yurui Chen, Chun Gu, Junzhe Jiang, Xiatian Zhu, and Li Zhang. Periodic vibration gaussian: Dynamic urban scene reconstruction and real-time rendering. *arXiv preprint*, 2023. 2, 3, 4, 7, 8, 14, 15
- [12] Zirui Wu, Tianyu Liu, Liyi Luo, Zhide Zhong, Jianteng Chen, Hongmin Xiao, Chao Hou, Haozhe Lou, Yuantao Chen, Runyi Yang, et al. Mars: An instance-aware, modular and realistic simulator for autonomous driving. In *CAAI*, 2023. 2
- [13] Jiawei Yang, Boris Ivanovic, Or Litany, Xinshuo Weng, Seung Wook Kim, Boyi Li, Tong Che, Danfei Xu, Sanja Fidler, Marco Pavone, et al. Emernerf: Emergent spatial-temporal scene decomposition via self-supervision. *arXiv preprint*, 2023. 2
- [14] Yunzhi Yan, Haotong Lin, Chenxu Zhou, Weijie Wang, Haiyang Sun, Kun Zhan, Xianpeng Lang, Xiaowei Zhou, and Sida Peng. Street gaussians for modeling dynamic urban scenes. In *ECCV*, 2024. 2, 3, 4, 5, 7, 8, 14
- [15] Ziyu Chen, Jiawei Yang, Jiahui Huang, Riccardo de Lutio, Janick Martinez Esturo, Boris Ivanovic, Or Litany, Zan Gojcic, Sanja Fidler, Marco Pavone, Li Song, and Yue Wang. Omnire: Omni urban scene reconstruction. *arXiv preprint*, 2024. 2, 3, 4, 5, 7, 8, 14
- [16] Haithem Turki, Jason Y Zhang, Francesco Ferroni, and Deva Ramanan. Suds: Scalable urban dynamic scenes. In *CVPR*, 2023. 2
- [17] Darren Robinson, Frédéric Haldi, Philippe Leroux, Diane Perez, Adil Rasheed, and Urs Wilke. Citysim: Comprehensive micro-simulation of resource flows for sustainable urban planning. In *IBPSA*, 2009. 2
- [18] U.S. Department of Transportation Federal Highway Administration. Next Generation Simulation (NGSIM) Vehicle Trajectories and Supporting Data, 2016. 2
- [19] Xiaosong Jia, Zhenjie Yang, Qifeng Li, Zhiyuan Zhang, and Junchi Yan. Bench2drive: Towards multi-ability benchmarking of closed-loop end-to-end autonomous driving. *arXiv preprint*, 2024. 2, 3

- [20] Daniel Dauner, Marcel Hallgarten, Tianyu Li, Xinshuo Weng, Zhiyu Huang, Zetong Yang, Hongyang Li, Igor Gilitschenski, Boris Ivanovic, Marco Pavone, Andreas Geiger, and Kashyap Chitta. Navsim: Data-driven non-reactive autonomous vehicle simulation and benchmarking. In *NeurIPS*, 2024. 2, 3, 6, 7, 8, 9, 14, 16
- [21] Pei Sun, Henrik Kretzschmar, Xerxes Dotiwalla, Aurelien Chouard, Vijaysai Patnaik, Paul Tsui, James Guo, Yin Zhou, Yuning Chai, Benjamin Caine, et al. Scalability in perception for autonomous driving: Waymo open dataset. In *CVPR*, 2020. 2, 3
- [22] Ruiyuan Gao, Kai Chen, Enze Xie, Lanqing Hong, Zhenguo Li, Dit-Yan Yeung, and Qiang Xu. Magicdrive: Street view generation with diverse 3d geometry control. *arXiv preprint*, 2023. 2
- [23] Xiaofeng Wang, Zheng Zhu, Guan Huang, Xinze Chen, and Jiwen Lu. Drivedreamer: Towards real-world-driven world models for autonomous driving. *arXiv preprint*, 2023. 2
- [24] Yunsong Zhou, Michael Simon, Zhenghao Peng, Sicheng Mo, Hongzi Zhu, Minyi Guo, and Bolei Zhou. Simgen: Simulator-conditioned driving scene generation. *arXiv preprint*, 2024. 2
- [25] Jianbo Zhao, Jiaheng Zhuang, Qibin Zhou, Taiyu Ban, Ziyao Xu, Hangning Zhou, Junhe Wang, Guoan Wang, Zhiheng Li, and Bin Li. Kigras: Kinematic-driven generative model for realistic agent simulation. *arXiv preprint*, 2024. 2
- [26] Wei Wu, Xiaoxin Feng, Ziyang Gao, and Yuheng Kan. Smart: Scalable multi-agent real-time simulation via next-token prediction. *arXiv preprint*, 2024. 2
- [27] Daniel Bogdoll, Yitian Yang, and J Marius Zöllner. Muvo: A multimodal generative world model for autonomous driving with geometric representations. *arXiv preprint*, 2023. 2
- [28] Shenyuan Gao, Jiazhi Yang, Li Chen, Kashyap Chitta, Yihang Qiu, Andreas Geiger, Jun Zhang, and Hongyang Li. Vista: A generalizable driving world model with high fidelity and versatile controllability. *arXiv preprint*, 2024. 2
- [29] Anthony Hu, Lloyd Russell, Hudson Yeo, Zak Murez, George Fedoseev, Alex Kendall, Jamie Shotton, and Gianluca Corrado. Gaia-1: A generative world model for autonomous driving. *arXiv preprint*, 2023. 2
- [30] Cole Gulino, Justin Fu, Wenjie Luo, George Tucker, Eli Bronstein, Yiren Lu, Jean Harb, Xinlei Pan, Yan Wang, Xiangyu Chen, et al. Waymax: An accelerated, data-driven simulator for large-scale autonomous driving research. In *NeurIPS*, 2024. 2, 3
- [31] Daniel Krajzewicz, Jakob Erdmann, Michael Behrisch, and Laura Bieker. Recent development and applications of sumo-simulation of urban mobility. *International journal on advances in systems and measurements*, 2012. 2
- [32] Licheng Wenl, Daocheng Fu, Song Mao, Pinlong Cai, Min Dou, Yikang Li, and Yu Qiao. Limsim: A long-term interactive multi-scenario traffic simulator. In *ITSC*, 2023. 2
- [33] Davis Rempe, Jonah Philion, Leonidas J Guibas, Sanja Fidler, and Or Litany. Generating useful accident-prone driving scenarios via a learned traffic prior. In *CVPR*, 2022. 2
- [34] Quanyi Li, Zhenghao Peng, Lan Feng, Qihang Zhang, Zhenghai Xue, and Bolei Zhou. Metadrive: Composing diverse driving scenarios for generalizable reinforcement learning. *IEEE TPAMI*, 2022. 2, 3
- [35] Ze Yang, Yun Chen, Jingkan Wang, Sivabalan Manivasagam, Wei-Chiu Ma, Anqi Joyce Yang, and Raquel Urtasun. Unisim: A neural closed-loop sensor simulator. In *CVPR*, 2023. 2
- [36] Guohang Yan, Jiahao Pi, Jianfei Guo, Zhaotong Luo, Min Dou, Nianchen Deng, Qiusheng Huang, Daocheng Fu, Licheng Wen, Pinlong Cai, et al. Oasim: an open and adaptive simulator based on neural rendering for autonomous driving. *arXiv preprint*, 2024. 2
- [37] William Ljungbergh, Adam Tonderski, Joakim Johnander, Holger Caesar, Kalle Åström, Michael Felsberg, and Christoffer Petersson. Neurorcap: Photorealistic closed-loop safety testing for autonomous driving. In *ECCV*, 2024. 2, 3, 4
- [38] Xuemeng Yang, Licheng Wen, Yukai Ma, Jianbiao Mei, Xin Li, Tiantian Wei, Wenjie Lei, Daocheng Fu, Pinlong Cai, Min Dou, et al. Drivearena: A closed-loop generative simulation platform for autonomous driving. *arXiv preprint*, 2024. 2, 3, 4
- [39] Hongyu Zhou, Longzhong Lin, Jiabao Wang, Yichong Lu, Dongfeng Bai, Bingbing Liu, Yue Wang, Andreas Geiger, and Yiyi Liao. Hugsim: A real-time, photo-realistic and closed-loop simulator for autonomous driving. *arXiv preprint*, 2024. 2, 5

- [40] Sergio Casas, Abbas Sadat, and Raquel Urtasun. Mp3: A unified model to map, perceive, predict and plan. In *CVPR*, 2021. 2
- [41] Shengchao Hu, Li Chen, Penghao Wu, Hongyang Li, Junchi Yan, and Dacheng Tao. St-p3: End-to-end vision-based autonomous driving via spatial-temporal feature learning. In *ECCV*, 2022. 2, 7, 8, 9
- [42] Kashyap Chitta, Aditya Prakash, Bernhard Jaeger, Zehao Yu, Katrin Renz, and Andreas Geiger. Transfuser: Imitation with transformer-based sensor fusion for autonomous driving. *IEEE TPAMI*, 2023. 2, 7, 8, 9, 15, 16, 17
- [43] Bo Jiang, Shaoyu Chen, Qing Xu, Bencheng Liao, Jiajie Chen, Helong Zhou, Qian Zhang, Wenyu Liu, Chang Huang, and Xinggang Wang. Vad: Vectorized scene representation for efficient autonomous driving. In *ICCV*, 2023. 2, 7, 8, 9
- [44] Diankun Zhang, Guoan Wang, Runwen Zhu, Jianbo Zhao, Xiwu Chen, Siyu Zhang, Jiahao Gong, Qibin Zhou, Wenyuan Zhang, Ningzi Wang, et al. Sparsead: Sparse query-centric paradigm for efficient end-to-end autonomous driving. *arXiv preprint*, 2024. 3
- [45] Wenchao Sun, Xuewu Lin, Yining Shi, Chuang Zhang, Haoran Wu, and Sifa Zheng. Sparsedrive: End-to-end autonomous driving via sparse scene representation. *arXiv preprint*, 2024. 3
- [46] Bencheng Liao, Shaoyu Chen, Haoran Yin, Bo Jiang, Cheng Wang, Sixu Yan, Xinbang Zhang, Xiangyu Li, Ying Zhang, Qian Zhang, et al. Diffusiondrive: Truncated diffusion model for end-to-end autonomous driving. In *CVPR*, 2025. 3, 7, 8, 9, 15, 16, 17
- [47] Andreas Geiger, Philip Lenz, and Raquel Urtasun. Are we ready for autonomous driving? the kitti vision benchmark suite. In *CVPR*, 2012. 3
- [48] Bernhard Kerbl, Georgios Kopanas, Thomas Leimkühler, and George Drettakis. 3d gaussian splatting for real-time radiance field rendering. In *ACM TOG*, 2023. 3
- [49] Xiaoyu Zhou, Zhiwei Lin, Xiaojun Shan, Yongtao Wang, Deqing Sun, and Ming-Hsuan Yang. Driving-gaussian: Composite gaussian splatting for surrounding dynamic autonomous driving scenes. In *CVPR*, 2024. 3
- [50] Hongyu Zhou, Jiahao Shao, Lu Xu, Dongfeng Bai, Weichao Qiu, Bingbing Liu, Yue Wang, Andreas Geiger, and Yiyi Liao. Hugs: Holistic urban 3d scene understanding via gaussian splatting. In *CVPR*, 2024. 3
- [51] Sivabalan Manivasagam, Shenlong Wang, Kelvin Wong, Wenyuan Zeng, Mikita Sazanovich, Shuhan Tan, Bin Yang, Wei-Chiu Ma, and Raquel Urtasun. Lidarsim: Realistic lidar simulation by leveraging the real world. In *CVPR*, 2020. 3
- [52] Chenqi Li, Yuan Ren, and Bingbing Liu. Pegen: Point cloud generator for lidar simulation. In *ICRA*, 2023. 3
- [53] Tang Tao, Longfei Gao, Guangrun Wang, Peng Chen, Dayang Hao, Xiaodan Liang, Mathieu Salzmann, and Kaicheng Yu. Lidar-nerf: Novel lidar view synthesis via neural radiance fields. *arXiv preprint*, 2023. 3
- [54] Junge Zhang, Feihu Zhang, Shaochen Kuang, and Li Zhang. Nerf-lidar: Generating realistic lidar point clouds with neural radiance fields. In *AAAI*, 2024. 3
- [55] Zehan Zheng, Fan Lu, Weiyi Xue, Guang Chen, and Changjun Jiang. Lidar4d: Dynamic neural fields for novel space-time view lidar synthesis. In *CVPR*, 2024. 3
- [56] Weiyi Xue, Zehan Zheng, Fan Lu, Haiyun Wei, Guang Chen, and Changjun Jiang. Geonlf: Geometry guided pose-free neural lidar fields. *arXiv preprint*, 2024. 3
- [57] Tang Tao, Guangrun Wang, Yixing Lao, Peng Chen, Jie Liu, Liang Lin, Kaicheng Yu, and Xiaodan Liang. Alignmif: Geometry-aligned multimodal implicit field for lidar-camera joint synthesis. In *CVPR*, 2024. 3
- [58] Hanfeng Wu, Xingxing Zuo, Stefan Leutenegger, Or Litany, Konrad Schindler, and Shengyu Huang. Dynamic lidar re-simulation using compositional neural fields. In *CVPR*, 2024. 3
- [59] Ben Mildenhall, Pratul P Srinivasan, Matthew Tancik, Jonathan T Barron, Ravi Ramamoorthi, and Ren Ng. Nerf: Representing scenes as neural radiance fields for view synthesis. In *ECCV*, 2020. 3
- [60] Junzhe Jiang, Chun Gu, Yurui Chen, and Li Zhang. Gs-lidar: Generating realistic lidar point clouds with panoramic gaussian splatting. In *ICLR*, 2025. 3, 4, 15, 16

- [61] Chenxu Zhou, Lvchang Fu, Sida Peng, Yunzhi Yan, Zhanhua Zhang, Yong Chen, Jiazhi Xia, and Xiaowei Zhou. LiDAR-RT: Gaussian-based ray tracing for dynamic lidar re-simulation. In *CVPR*, 2025. 3, 4
- [62] Georg Hess, Carl Lindström, Maryam Fatemi, Christoffer Petersson, and Lennart Svensson. Splatad: Real-time lidar and camera rendering with 3d gaussian splatting for autonomous driving. *arXiv preprint*, 2024. 4
- [63] Haoqiang Fan, Hao Su, and Leonidas J Guibas. A point set generation network for 3d object reconstruction from a single image. In *CVPR*, 2017. 5
- [64] Zeyu Yang, Zijie Pan, Yuankun Yang, Xiatian Zhu, and Li Zhang. Driving scene synthesis on free-form trajectories with generative prior. *arXiv preprint*, 2024. 5, 15, 16
- [65] Wangbo Yu, Jinbo Xing, Li Yuan, Wenbo Hu, Xiaoyu Li, Zhipeng Huang, Xiangjun Gao, Tien-Tsin Wong, Ying Shan, and Yonghong Tian. Viewcrafter: Taming video diffusion models for high-fidelity novel view synthesis. *arXiv preprint*, 2024. 5, 15
- [66] Zhiwen Yan, Weng Fei Low, Yu Chen, and Gim Hee Lee. Multi-scale 3d gaussian splatting for anti-aliased rendering. In *CVPR*, 2024. 5
- [67] Zehao Yu, Anpei Chen, Binbin Huang, Torsten Sattler, and Andreas Geiger. Mip-splatting: Alias-free 3d gaussian splatting. In *CVPR*, 2024. 5
- [68] Xiaowei Song, Jv Zheng, Shiran Yuan, Huan-ang Gao, Jingwei Zhao, Xiang He, Weihao Gu, and Hao Zhao. Sa-gs: Scale-adaptive gaussian splatting for training-free anti-aliasing. *arXiv preprint*, 2024. 5
- [69] Jeremy Reizenstein, Roman Shapovalov, Philipp Henzler, Luca Sbordone, Patrick Labatut, and David Novotny. Common objects in 3d: Large-scale learning and evaluation of real-life 3d category reconstruction. In *ICCV*, 2021. 5, 7, 17
- [70] Xiaobiao Du, Haiyang Sun, Shuyun Wang, Zhuojie Wu, Hongwei Sheng, Jiaying Ying, Ming Lu, Tianqing Zhu, Kun Zhan, and Xin Yu. 3drealcar: An in-the-wild rgb-d car dataset with 360-degree views. *arXiv preprint*, 2024. 5, 7, 17
- [71] Zian Wang, Tianchang Shen, Jun Gao, Shengyu Huang, Jacob Munkberg, Jon Hasselgren, Zan Gojcic, Wenzheng Chen, and Sanja Fidler. Neural fields meet explicit geometric representations for inverse rendering of urban scenes. In *CVPR*, 2023. 5
- [72] Robin Rombach, Andreas Blattmann, Dominik Lorenz, Patrick Esser, and Björn Ommer. High-resolution image synthesis with latent diffusion models. In *CVPR*, 2022. 6
- [73] Ben Poole, Ajay Jain, Jonathan T Barron, and Ben Mildenhall. Dreamfusion: Text-to-3d using 2d diffusion. *arXiv preprint*, 2022. 6
- [74] Sketchfab Contributors. Sketchfab. <https://sketchfab.com/>. 7
- [75] OpenScene Contributors. Openscene: The largest up-to-date 3d occupancy prediction benchmark in autonomous driving. <https://github.com/OpenDriveLab/OpenScene>, 2023. 7
- [76] Shubhankar Borse, Ying Wang, Yizhe Zhang, and Fatih Porikli. Inverseform: A loss function for structured boundary-aware segmentation. In *CVPR*, 2021. 8
- [77] Enze Xie, Wenhai Wang, Zhiding Yu, Anima Anandkumar, Jose M Alvarez, and Ping Luo. Segformer: Simple and efficient design for semantic segmentation with transformers. In *NeurIPS*, 2021. 8
- [78] Tianhe Ren, Shilong Liu, Ailing Zeng, Jing Lin, Kunchang Li, He Cao, Jiayu Chen, Xinyu Huang, Yukang Chen, Feng Yan, Zhaoyang Zeng, Hao Zhang, Feng Li, Jie Yang, Hongyang Li, Qing Jiang, and Lei Zhang. Grounded sam: Assembling open-world models for diverse visual tasks. *arXiv preprint*, 2024. 8
- [79] Binbin Huang, Zehao Yu, Anpei Chen, Andreas Geiger, and Shenghua Gao. 2d gaussian splatting for geometrically accurate radiance fields. In *SIGGRAPH*, 2024. 15

A Urban scene reconstruction

A.1 NuPlan pose correction

We propose a pose correction method based on LiDAR point cloud registration in Section 3.1.1. As shown in Figure 7, point cloud registration effectively corrects pose calibration errors. This leads to improved scene reconstruction quality, which is reflected in the increased PSNR, as presented in Table 5.

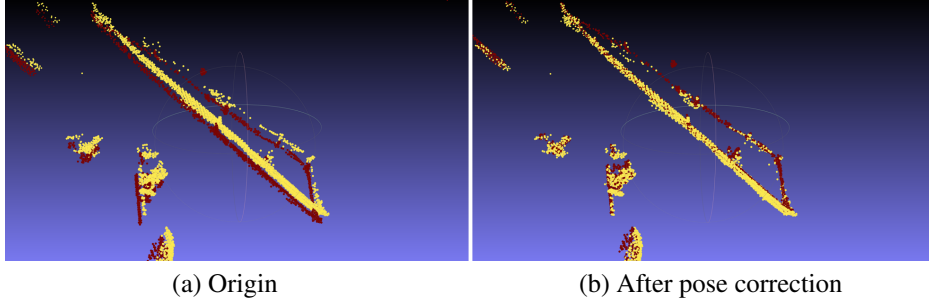


Figure 7: **Pose correction in nuPlan.** The yellow and red points originate from LiDAR point clouds of different frames. (a) Due to the coarse pose calibration in nuPlan, LiDAR point clouds from different frames are misaligned in the world coordinate system, posing challenges for high-quality reconstruction. (b) After our pose correction, LiDAR point clouds are properly aligned, leading to improved camera images reconstruction quality.

Table 5: Ablation study on camera images reconstruction in the nuPlan benchmark.

	PSNR↑	SSIM↑	LPIPS↓
w/o \mathcal{L}_{cd}	26.02	0.798	0.179
w/o undistortion	25.68	0.809	0.182
w/o color correction	28.05	0.853	0.132
RealEngine(Ours)	29.67	0.897	0.093

A.2 Camera images reconstruction

We use StreetGaussians [14] to reconstruct the scene and perform additional processing on the nuPlan dataset. StreetGaussians [14] uses manual pose annotation of dynamic objects to distinguish between static background and moving objects. Dynamic objects are reconstructed in their respective centered canonical spaces and then placed into the background scene space during the rendering process based on the known poses.

As shown in Figure 8 (a), the camera images in nuPlan exhibit significant barrel distortion. Since 3DGS relies on image-based rendering and does not render rays corresponding to each pixel as NeRF does, such distortion adversely affects the reconstruction of scene geometry. To mitigate this issue, we applied a distortion correction to the images. Furthermore, due to varying exposure levels across the cameras in the nuPlan dataset, the same object exhibits substantial color differences when viewed from different cameras, as shown in Figure 8 (b), leading to ambiguities in the color information of Gaussian primitives. To address this, we introduced a learnable affine transformation $\{A_i, t_i\}$ for each camera i to individually calibrate the image colors:

$$\tilde{C}_i = A_i C_i + t_i \quad (6)$$

where i represents the camera index, C_i denotes the original rendered RGB map, and \tilde{C}_i refers to the RGB map after exposure transformation. These processing methods improve the quality of scene reconstruction, as shown in the ablation study in Table 5.

We compared our optimized reconstruction results with the state-of-the-art methods [14, 15, 11] on 6 Navsim [20] sequences, as shown in Figure 3 and Table 3, and observed a notable improvement in the reconstruction performance on nuPlan.



Figure 8: **Distortion and color inconsistency in the nuPlan benchmark.** (a) The camera images in nuPlan exhibit significant barrel distortion, which poses challenges for Gaussian splatting based reconstruction. To address this, we apply distortion correction to the images. (b) Additionally, different cameras have varying exposure levels. To prevent color ambiguity for the same Gaussian primitive across different cameras, we learn an exposure transformation for each camera separately.

Although existing urban reconstruction methods perform excellently in synthesizing novel viewpoints for recorded trajectories, they face challenges when handling new trajectories in closed-loop simulations due to the limited viewpoints of driving videos and the vastness of the driving environment. To address this challenge, we employ DriveX [64] to enhance the reconstructed scene, which utilizes video generative prior [65] to optimize the scene model across multiple trajectories. As shown in Figure 9, our final scene model is capable of generating high-fidelity virtual driving environments beyond the recorded trajectories, enabling free-form trajectory driving simulations.

A.3 LiDAR reconstruction

Table 6: Evaluation of LiDAR reconstruction performance in the nuPlan benchmark.

	Point Cloud	Depth		Intensity	
	CD↓	RMSE↓	PSNR↑	RMSE↓	PSNR↑
GS-LiDAR [60]	0.315	6.930	21.25	0.0903	20.88

We use GS-LiDAR [60] to reconstruct the LiDAR point clouds. GS-LiDAR [60] introduces a novel panoramic rendering technique with explicit ray-splat intersection, guided by panoramic LiDAR supervision. This method employs 2D Gaussian primitives [79] with periodic vibration characteristics [11], allowing for precise geometric reconstruction of both static and dynamic elements in driving scenes.

The LiDAR point clouds in nuPlan [7] is generated by merging point clouds from five LiDAR sensors, with non-uniform angular distributions across different scan lines. However, GS-LiDAR assumes that the LiDAR point cloud originate from a single laser scanner with uniformly spaced scan lines. To address this discrepancy, we reproject the merged point cloud onto the top LiDAR sensor to obtain the range map, selecting the point with the smaller depth when multiple points project to the same pixel. Additionally, we discard the non-uniform scan lines at both ends while retaining the central region, where the scan lines are evenly distributed.

As shown in Figure 10, this processing method results in some loss of LiDAR information. However, since the driving agent [42, 46] converts the LiDAR point cloud into a 2-bin histogram over a 2D BEV grid with relatively low resolution, the missing information has a minimal impact on the driving agent. We evaluate the reconstruction performance on the same 6 sequences as the camera image reconstruction in Table 6.



Figure 9: **Lane change reconstruction.** We render the camera images by shifting the driving perspective 3 meters to the left and right. Due to the limited viewpoint of driving videos and the vastness of the driving environment, large translations from driving perspectives lead to a significant decline in reconstruction quality. To address this, we use DriveX [64], which leverages video generative prior to optimize the scene Gaussian primitives, resulting in improved reconstruction quality even with large viewpoint translations.

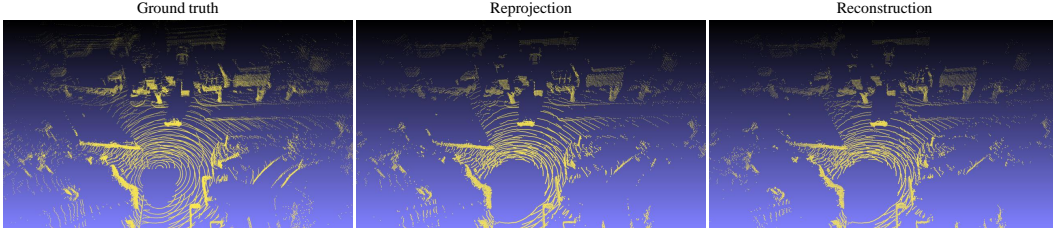


Figure 10: **LiDAR reconstruction.** Although reprojection may lead to some loss of LiDAR information, its impact on the low-resolution histogram used by the agent is minimal. Meanwhile, GS-LiDAR [60] achieves high-quality reconstruction of the reprojected LiDAR data.

B Consistency of driving behaviors

We replicate the same real-world evaluation scenarios from the Navsim [20] benchmark in the non-reactive open-loop setting in Table 2, and evaluate autonomous driving models [42, 46] trained solely on real data in both the real open-loop environment and its simulated counterpart in RealEngine, comparing the performance differences.

We use the the Predictive Driver Model Score (PDMS) [20] between trajectories as a measure of similarity, and conduct evaluations only on sequences where the PDMS is greater than zero. The gap is defined as follows:

$$\text{gap} = \frac{|\text{PDMS}_{\text{real}} - \text{PDMS}_{\text{sim}}|}{\max(\text{PDMS}_{\text{real}}, \text{PDMS}_{\text{sim}})} \quad (7)$$

Specifically, $\text{PDMS}_{\text{real}}$ refers to the PDMS of the trajectory planned based on real sensor inputs, whereas PDMS_{sim} corresponds to that planned using sensor data simulated by RealEngine. To evaluate the realism of camera and LiDAR simulation independently, we test three settings: (i) simulating only the camera (PDMS_{cam}), (ii) simulating only the LiDAR ($\text{PDMS}_{\text{lidar}}$), and (iii) simulating both camera and LiDAR ($\text{PDMS}_{\text{both}}$), as shown in Table 7. To better understand the realism of RealEngine, we also visualize the trajectories planned by DiffusionDrive [46], as shown in Figure 11.

Table 7: **Consistency of driving behaviors.** We test Transfuser [42] and DiffusionDrive [46], which take camera and LiDAR inputs, under the three settings described in Appendix B.

Method	Image	LiDAR	$\text{PDMS}_{\text{real}} \uparrow$	$\text{PDMS}_{\text{cam}} \uparrow$	$\text{gap}_{\text{cam}} \downarrow$	$\text{PDMS}_{\text{lidar}} \uparrow$	$\text{gap}_{\text{lidar}} \downarrow$	$\text{PDMS}_{\text{both}} \uparrow$	$\text{gap}_{\text{both}} \downarrow$
Transfuser [42]	✓	✓	81.18	80.99	0.77%	80.78	0.55%	80.56	0.98%
DiffusionDrive [46]	✓	✓	80.75	81.07	0.89%	80.85	0.42%	81.07	1.07%

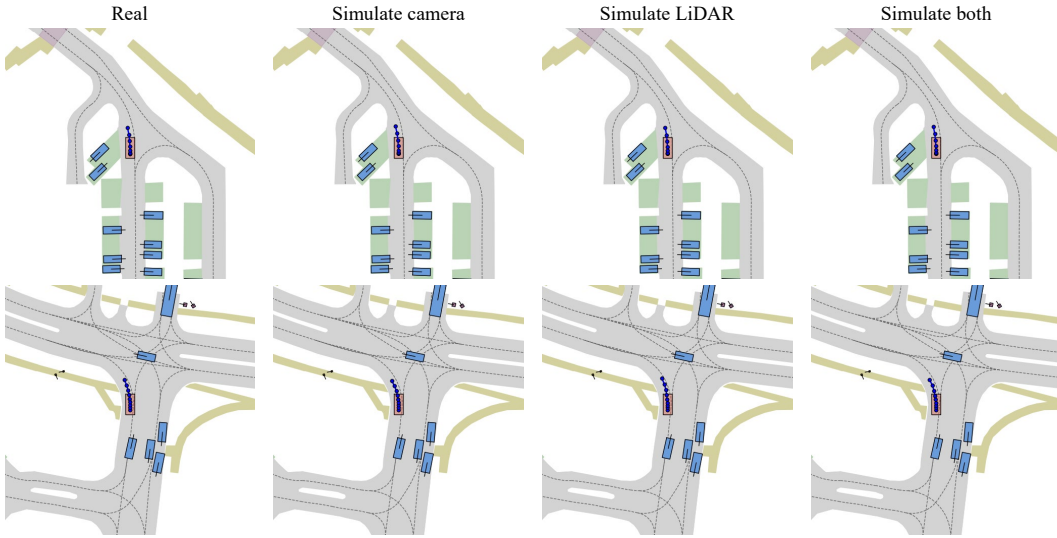


Figure 11: **Consistency of driving behaviors.** We test DiffusionDrive [46] under the same settings in Table 7. The close alignment between trajectories in the real and simulated environments demonstrates the high fidelity of our RealEngine.

The results show that the planned trajectory gap between the real-world environment and the counterpart simulated by RealEngine remains small (approximately 1%), which highlights the realism of our simulator and its effectiveness in supporting closed-loop evaluation of autonomous driving models.

C Limitations

We still have a few limitations for future improvement:

Firstly, our current foreground meshes rely on existing datasets [69, 70] and 3D asset libraries, which limits the diversity of the foreground. We plan to incorporate generative models to generate foreground objects, thereby reducing manual effort, enhancing the richness of the scenes, and improving the generalizability of the simulation platform.

Secondly, although we have relighting models, there are still noticeable differences between the inserted traffic participants and the background scene. To address this issue, we plan to continuously track and integrate state-of-the-art advancements in foreground insertion to ensure seamless blending of traffic participants with the background.

Thirdly, we employ a simplified vehicle model that does not account for aerodynamic effects, suspension, or tire characteristics. Additionally, we overlook substantial variations in road conditions, such as changes in friction coefficients (e.g., wet or icy surfaces), gradients, and irregularities.